Nuclear orientation in the reaction $^{34}S + ^{238}U$ and synthesis of the new isotope ^{268}Hs

K. Nishio,[1] S. Hofmann,[2,3] F. P. Heßberger,[2] D. Ackermann,[2] S. Antalic,[4] Y. Aritomo,[1,5] V. F. Comas,[6] Ch. E. Düllmann,[2] A. Gorshkov,[7] R. Graeger,[7] K. Hagino,[8] S. Heinz,[2] J. A. Heredia,[2] K. Hirose,[9] H. Ikezoe,[1] J. Khuyagbaatar,[2] B. Kindler,[2] I. Kojouharov,[2] B. Lommel,[2] R. Mann,[2] S. Mitsuoka,[1] Y. Nagame,[1] I. Nishinaka,[1] T. Ohtsuki,[9] A. G. Popeko,[5] S. Saro,[4] M. Schädel,[2] A. Türler,[7] Y. Watanabe,[10] A. Yakushev,[7] and A. V. Yeremin[5]

[1]*Japan Atomic Energy Agency, Tokai, Ibaraki 319-1195, Japan*
[2]*GSI Helmholtzzentrum für Schwerionenforschung, D-64291 Darmstadt, Germany*
[3]*Institut für Kernphysik, Goethe-Universität Frankfurt, D-60438 Frankfurt am Main, Germany*
[4]*Department of Nuclear Physics and Biophysics, Comenius University, SK-84248 Bratislava, Slovakia*
[5]*Flerov Laboratory of Nuclear Reactions, 141 980 Dubna, Russia*
[6]*Higher Institute of Technologies and Applied Sciences, Habana 10400, Cuba*
[7]*Institut für Radiochemie, Technische Universität München, D-85748 Garching, Germany*
[8]*Department of Physics, Tohoku University, Sendai 980-8597, Japan*
[9]*Laboratory of Nuclear Science, Tohoku University, Sendai 982-0826, Japan*
[10]*High Energy Accelerator Organization (KEK), Tsukuba 305-0801, Japan*

(Received 2 July 2010; published 31 August 2010)

The synthesis of isotopes of the element hassium was studied using the reaction $^{34}S + ^{238}U \rightarrow ^{272}Hs^*$. At a kinetic energy of 163.0 MeV in the center-of-mass system we observed one α-decay chain starting at the isotope ^{267}Hs. The cross section was $1.8^{+4.2}_{-1.5}$ pb. At 152.0 MeV one decay of the new isotope ^{268}Hs was observed. It decays with a half-life of $0.38^{+1.8}_{-0.17}$ s by 9479 $\pm$ 16 keV α-particle emission. Spontaneous fission of the daughter nucleus ^{264}Sg was confirmed. The measured cross section was $0.54^{+1.3}_{-0.45}$ pb. In-beam measurements of fission-fragment mass distributions were performed to obtain information on the fusion probability at various orientations of the deformed target nucleus. The distributions changed from symmetry to asymmetry when the beam energy was changed from above-barrier to sub-barrier values, indicating orientation effects on fusion and/or quasifission. It was found that the distribution of symmetric mass fragments originates not only from fusion-fission, but has a strong component from quasifission. The result was supported by a calculation based on a dynamical description using the Langevin equation, in which the mass distributions for fusion-fission and quasifission fragments were separately determined.

DOI: 10.1103/PhysRevC.82.024611 PACS number(s): 25.70.Jj, 23.60.+e, 25.70.Gh, 27.90.+b

I. INTRODUCTION

A striking feature in the production of superheavy nuclei (SHN) is that, in reactions based on targets of actinides and ^{48}Ca beams, the cross sections maintain values of a few picobarns even for the production of the heaviest elements [1]. This feature of the so-called hot-fusion reactions differs from results observed in cold-fusion reactions based on lead and bismuth targets, which revealed that cross sections continuously decrease with increasing atomic number [2,3]. These relatively large cross sections measured in the hot-fusion reactions are explained by a high survival probability of the compound nuclei in competition with fission owing to large fission barriers of nuclei in the vicinity of the $N = 184$ shell closure. An additional reason could be a higher fusion probability in reactions using actinide targets. Because actinide nuclei are prolately deformed, there exists a configuration at which the projectiles hit the equatorial region of the deformed target nuclei. In this case, a compact configuration is achieved and the system may have a larger fusion probability than in reactions using spherical target nuclei, such as lead or bismuth. In lighter systems that lead to actinide compound nuclei, reactions with the deformed nuclei of rare-earth elements had higher fusion probabilities at energies in which equatorial collisions occur than those with spherical target nuclei [4,5]. Also in heavier systems, as for example in the production of seaborgium isotopes using the reaction $^{30}Si + ^{238}U$, no significant reduction of the fusion cross section owing to an increased Coulomb reseparation of the reaction partners in the entrance channel was measured [6]. In the present study we investigated the fusion and evaporation residue (ER) cross sections for the reaction $^{34}S + ^{238}U$, having larger repulsive Coulomb forces owing to an increase in the projectile charge compared to the system $^{30}Si + ^{238}U$.

In fusion reactions with very asymmetric systems, the effects of Coulomb reseparation are expected to be small or even negligible owing to the prevailing strength of attractive surface tension. Therefore, in reactions with actinide targets, fusion also occurs at low beam energies in polar collisions owing to the low Coulomb barrier in this configuration. At the resulting lower excitation energy of the compound nucleus, fewer neutrons are evaporated and more neutron-rich ERs can be produced. In the reaction $^{16}O + ^{238}U$ the measured ER cross section for the $4n$ channel is significantly larger at sub-barrier energies than those obtained from a statistical model calculation based on a one-dimensional barrier penetration model for fusion [7]. Therefore, sub-barrier fusion has been exploited for the production of SHN isotopes by $3n$ or $4n$ evaporation. Examples are $^{261,260}Rf$ produced in reactions of

^{26}Mg + ^{238}U [8], ^{264}Sg in ^{30}Si + ^{238}U [6,9], and ^{270,271}Hs in ^{26}Mg + ^{248}Cm [10,11].

In the presented study, we were aiming to produce the new isotope ^{268}Hs in the 4*n* channel in sub-barrier fusion of ^{34}S + ^{238}U. At higher beam energy, the lighter isotope ^{267}Hs can be produced in the 5*n* channel. This isotope was first observed as a daughter nucleus in the decay chain of ^{271}Ds [12,13]. Production of ^{267}Hs in the reaction ^{34}S + ^{238}U was reported in Ref. [14]. Our strategy was to first confirm the production of ^{267}Hs in the 5*n* channel at a beam energy above the barrier and then to decrease the beam energy for the production of the new isotope ^{268}Hs. An estimate for the optimum yield to produce ^{268}Hs resulted in an excitation energy 11 MeV less than that needed to produce ^{267}Hs, as explained in Sec. IV.

In addition to the investigation of separated ERs from complete fusion reactions, we studied the mass distribution of fission fragments with in-beam measurement at energies below and above the barrier. In this experiment we were aiming to receive information on the fusion probability at various orientations of the deformed target nucleus.

II. EXPERIMENTAL DETAILS

A. Evaporation residue measurement

The experiments were performed at the linear accelerator UNILAC and the velocity filter SHIP at GSI in Darmstadt. A $^{34}S^{5+}$ beam was extracted from a 14-GHz ECR ion source using $^{34}SO_2$ with a 99% isotopic enrichment. Average beam intensities at the target position were typically 2.0–2.5 $p\mu$A (particle μA). The beam had a pulse structure of 5.0 ms width at 50 Hz repetition frequency. The SHIP setup was essentially the same as described in Ref. [2].

The uranium targets were prepared by sputtering of depleted ^{238}U metal on a 43 μg/cm^2 carbon backing. The target layers were 412–439 μg/cm^2 thick. The uranium layers were coated with a 10-μg/cm^2-thick carbon layer to prevent loss of material owing to sputtering and to prevent oxidation. During the run, the thickness of the uranium layer was occasionally monitored using scattering of 20-keV electrons [15]. We also monitored the target thickness by continuously registering the number of elastically scattered projectiles normalized to the beam current. The reaction energy in the center-of-mass system at the front and rear surface of the ^{238}U layer was 1.0 MeV higher and lower, respectively, than the energy in the center of the target owing to energy loss of the beam particles. A 30 μg/cm^2 carbon foil was installed at a distance of 160 mm downstream from the target to bring the ionic charge state of the ERs into equilibrium. The efficiency of SHIP was estimated to be 15% according to a Monte Carlo simulation.

In the focal plane of SHIP, ERs and their subsequent α decay and/or spontaneous fission (sf) were detected by a position sensitive 16-strip Si PIPS detector (stop detector) with an active area of 80 × 35 mm. Escaping α particles or fission fragments were detected by a "box detector," which covered 85% of the area of the backward hemisphere. Timing detectors were located in front of the silicon detector array to distinguish signals from implanted ERs or background particles from radioactive decays in the stop detector. In the irradiation at 5.53 MeV/u beam energy for producing ^{267}Hs, only one timing detector was used. In the irradiation at 5.16 MeV/u for producing ^{268}Hs, a second timing detector was added. Details of the timing detector are described in Ref. [16]. The secondary electrons are generated by a thin carbon foil of 30 μg/cm^2 thickness. The electric field used to accelerate the electrons is formed between the carbon foil and a grid plane made from gilded tungsten wires 20 μm in diameter separated by a distance of 3 mm.

A low-energy branch with an energy range of 0.1–16 MeV was used to measure implanted ERs and α decays. It was calibrated using α rays from ^{203,204,205}Fr, ^{203,204,205}Rn, ^{200,201}At, and ^{200}Po produced by irradiating a ^{nat}Lu target. The energy resolution for α particles fully stopped in the stop detector was typically 26 keV [full width at half maximum (FWHM)]. For α particles escaping with an energy loss, ΔE, from the stop detector and being detected with a residual energy, E_{res}, in one of the box detector, the resolution for the total energy, $E = \Delta E + E_{res}$, depended on a combination of the position in a particular strip of the stop detector and the box-detector segment. The mean value was 70 keV (FWHM).

The high-energy branch, with an energy range of 3–320 MeV for the detection of fission fragments, was calibrated using external α-particle sources and beam particles passing SHIP as background. The total kinetic energy (TKE) of sf events was obtained by summing the energies from the stop and the box detectors. The high-energy branch of the box detector was calibrated using external α sources.

An energy correction was performed to take into account energy losses owing to electron-hole recombination and losses in the inactive detector surfaces. The necessary calibration curves were obtained from measurements of the sf of ^{252}No whose TKE is known and analyzed as a function of the implantation depth in the stop detector [17,18]. The implantation depth of ^{268}Hs at 5.16 MeV/u beam energy was calculated to be 2.9 μm. An energy deficit of 46 MeV was obtained, which was added to the measured energy of the fission fragments to determine the TKE values.

A clover detector consisting of four Ge crystals (Ge1–Ge4) was mounted behind the stop detector. Each crystal had a diameter of 50 mm and a length of 70 mm. This detector was used to measure γ rays or x rays accompanied by α decay and/or sf. Owing to the high multiplicity of γ rays emitted from sf fragments, the detection of γ rays in coincidence with fission fragments provides strong evidence for the occurrence of true sf events. In the case of ^{252}No, 90% of the sf events generated signals in at least one of the Ge crystals.

The detection of correlated events is primarily based on a coincidence of the positions of implanted ER, subsequent α decays, and/or sf. From the measured position resolution determined in Ref. [6], we imposed the condition that at least one of the positions measured from the top and bottom of the detector strip agrees to within ±1.0 mm for the correlations of α_1-α_2 and ER-α. An agreement within ±1.2 mm was required for the ER-sf and α-sf correlations. For escaping α particles with energy of less than 3000 keV, an agreement of ±1.5 mm was imposed. We searched implanted ERs in the energy window of 4.0 MeV < E_{recoil} < 15.0 MeV as a possibly detectable range.

B. In-beam fission measurement

Prior to the synthesis of hassium isotopes at the GSI SHIP, we had measured the mass distributions and cross sections of fragments emerging from the reaction $^{34}S + ^{238}U \rightarrow ^{272}Hs^*$. This investigation was carried out at the tandem accelerator of the Japan Atomic Energy Agency (JAEA) in Tokai. The experimental setup and the analysis method were the same as in our previous study of the reaction $^{36}S + ^{238}U \rightarrow ^{274}Hs^*$ [19].

Beam energies were changed in the range 160–204 MeV ^{34}S to measure the energy dependence of fragment mass distributions, as well as fission cross section. Typical beam intensities were from 0.1 to 1.0 *p*nA. The ^{238}U target was prepared by electrodeposition of UO_2 on a 90-μ g/cm^2-thick Ni backing. The ^{238}U target was 82 μg/cm^2 thick. Both fission fragments were detected in coincidence by position-sensitive multiwire proportional counters (MWPCs). The detectors were located on both sides of the target each at a distance of 211 mm and at angles of $\theta_1 = -61.0^\circ$ for MWPC1 and $\theta_2 = +90.0^\circ$ for MWPC2. The MWPCs covered emission angles of $-86.0^\circ \leqslant \theta_1 \leqslant -36.0^\circ$ and $65.0^\circ \leqslant \theta_2 \leqslant 115.0^\circ$. The MWPC1 covered the out-of-plane angle of $72.0^\circ \leqslant \phi_1 \leqslant 108.0^\circ$ at $\theta_1 = -61^\circ$, and the MWPC2 covered the angle of $74.1^\circ \leqslant \phi_2 \leqslant 105.9^\circ$ at $\theta_2 = +90^\circ$ (for definition of the angles, see Ref. [19]).

The time difference, ΔT, between the signals from MWPC1 and MWPC2 was measured. The charges induced in both MWPCs contain information on the energy deposition ΔE_1 and ΔE_2 of particles traversing the detectors and were recorded. In the two-dimensional spectrum of ΔT versus $\Delta E_1 + \Delta E_2$, fission events were well separated from elastically scattered projectile-target events.

In the two-dimensional spectrum of $\theta_{12} = \theta_1 + \theta_2$ versus $\phi_{12} = \phi_1 + \phi_2$ fission events occurring after complete transfer of the projectile momentum to the composite system [full momentum transfer (FMT) fission] are separated from those fission events following nucleon transfer. These latter events occur when fissile targets like ^{238}U are irradiated.

For normalization of the beam current, a silicon surface barrier detector with a sold angle of 1.96 msr was mounted at 27.5° relative to the beam direction.

III. RESULTS FROM EVAPORATION RESIDUE MEASUREMENT

A. The isotope ^{267}Hs

In the irradiation for producing the isotope ^{267}Hs, a beam energy of 5.53 MeV/u was chosen. A beam dose of 4.8×10^{18} was accumulated. After passing through the carbon backing and half the length of the uranium layer, the beam energy became 186.3 MeV at the center of the target corresponding to a center-of-mass energy $E_{\mathrm{c.m.}}$ 163.0 MeV. The energy is higher than the Bass barrier of 159.3 MeV [20]. We used only one timing detector located at a distance of 245 mm from the stop detector. It had an efficiency of 98.9% for the detection of implanted particles in the energy between 7500 and 10500 keV, that is, in the range of α-decay energies of hassium isotopes and their decay products. Owing to the relatively low anticoincidence efficiency, we imposed the conditions that at least two α decays of the chain had to be detected during the beam-off period or that the decay chain terminated by sf for an unambiguous identification as a decay chain.

In this irradiation we observed a decay chain in strip No. 10, which we assign to the production of ^{267}Hs. The chain is shown in the upper part of Fig. 1. At 29.5 ms after a recoil implantation with 10.7 MeV, a first α decay was observed. The α particle escaped from the stop detector with an energy deposition of 665 keV and was absorbed in section No. 30 of the box detector. The sum of the two energy signals was 9993 keV. The assignment of strip numbers of the stop detector and of segment numbers of the box detector can be taken from Fig. 1 in Ref. [21].

From the geometry given by the positions in the stop and the box detector numbers, we determined an emission angle between 3° and 33° with respect to the surface plane of the stop detector for the escaped α particle. This value is in agreement with the emission angle of 24° determined from the calculated implantation depth of 2.9 μm and the length of 7.2 μm, traversed by the α particle in the stop detector before escaping. This latter length was obtained from the 665 keV deposited by the α particle.

The accuracy of the α-particle energy is 125 keV (FWHM) or $\sigma = \pm 50$ keV for this event and in this combination of strip

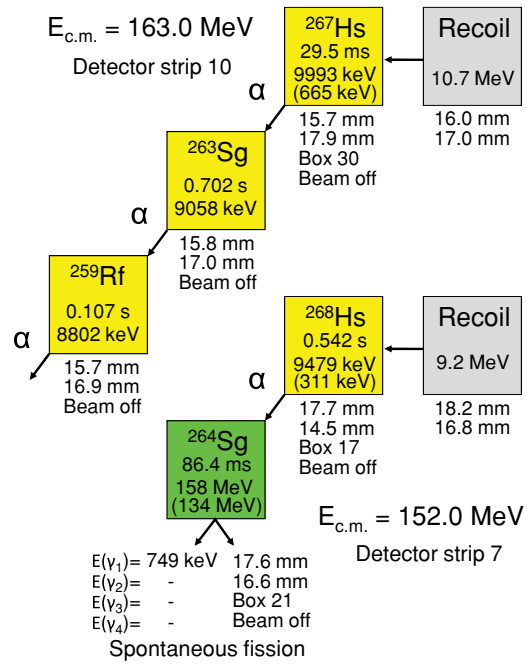

FIG. 1. (Color online) Decay chains observed in the $^{34}S + ^{238}U$ reaction at the center-of-mass energies of 163.0 and 152.0 MeV at the center of the target. The strip numbers of the stop detector are given. Data inside the boxes show the measured implantation energies, lifetimes, and total energies of α decays or sf. In the case of escaped particles, the energy deposition in the stop detector is given in parentheses. Below the boxes are given the vertical positions determined independently from the top and bottom signals of the strip, segment number of the box detector in the case of escaping particles, energies of coincident γ-ray event in the fourfold clover detector, and status of the beam in the case of radioactive decays.

and box-detector segments. This relatively low accuracy arises from the relatively large energy loss in the dead layer of the stop detector and the uncertainty of the emission angle.

The α decay of 9.99 ± 0.05 MeV assigned to the decay of ^{267}Hs is in agreement within error bars with the decay data of this isotope measured in the decay chain of ^{271}Ds. In 35 chains measured so far [13,22–25], the dominant α transition was at 9.88 ± 0.02 MeV. However, few events were also observed at energies in the range from 9.70 to 10.00 MeV [24].

In agreement within two standard deviations are also two of the three energies measured in the reaction $^{34}\mathrm{S} + ^{238}\mathrm{U}$, which were assigned to ^{267}Hs in Ref. [14]. The reported energies are 9.74, 9.86, and 9.87 MeV with error bars of ± 0.03 MeV.

The measured lifetime of 29.5 ms ($T_{1/2} = 20^{+98}_{-9}$ ms) agrees, to within the relatively large error bars for this one event, with the more accurate value of $T_{1/2} = 67^{+14}_{-10}$ ms determined from the 35 decay chains of ^{271}Ds. Note that we followed the error estimation in Ref. [26].

The first α decay was followed by a daughter decay with an energy of 9058 ± 11 keV at a lifetime of 0.702 s ($T_{1/2} = 0.49^{+2.3}_{-0.22}$ s).

This energy and half-life agree well with the decay of the lower energy transition of the two known long-lived states in ^{263}Sg having energies and half-lives of 9.06 MeV, $0.88^{+0.53}_{-0.24}$ s and 9.25 MeV, $0.56^{+0.14}_{-0.09}$ s, respectively. These mean values of the literature data were determined from studies of ^{263}Sg using the reactions $^{18}\mathrm{O} + ^{249}\mathrm{Cf}$ and $^{30}\mathrm{Si} + ^{238}\mathrm{U}$ [6,9,27,28], as well as from the decay of ^{263}Sg produced as granddaughter in the decay chain of ^{271}Ds [13,22–25].

For the energy and lifetime of the decay of ^{259}Rf, the granddaughter of ^{267}Hs, we measured values of 8802 ± 11 keV and 0.107 s ($T_{1/2} = 0.074^{+0.35}_{-0.034}$ s). Two α energies of 8.77 and 8.87 MeV are given in the literature for the decay of ^{259}Rf [29]. The energy of our event agrees with the lower energy transition. For this transition a half-life of $2.6^{+1.1}_{-0.58}$ s was determined from 12 events reported in Refs. [6,9,14,22,24,25]. The half-life measured for our event is considerably shorter. However, owing to the long tails of exponential time distributions, we still obtained a probability of 2.8% that the half-life of our event is in agreement with the literature value for ^{259}Rf. A comparably short lifetime of 0.41 s was measured in Ref. [24] for one of the ^{259}Rf decays of the chains from ^{271}Ds.

We searched for the decay of the great-granddaughter, ^{255}No, within a time window of ten times the half-life, 3.1 min [29], but no event was found. In this case it is very likely that the decay remained unobserved owing to the relatively high electron-capture branching of 38.6% of ^{255}No.

The production cross section for ^{267}Hs was determined to be $1.8^{+4.2}_{-1.5}$ pb, which agrees with the value of 2.5 pb given in Ref. [14].

B. The new isotope ^{268}Hs

In the second part of the experiment, we irradiated the uranium target with ^{34}S ions at 5.16 MeV/u energy, which resulted in $E_{\mathrm{c.m.}} = 152.0$ MeV at the center of the target. At this energy, a beam dose of 1.2×10^{19} was accumulated. One decay chain was identified, which is shown in the lower part of Fig. 1. The measured cross section was $0.54^{+1.3}_{-0.45}$ pb.

An α decay with an energy of 9479 keV was observed during the beam-off period. The α particle escaped from strip No. 7 of the stop detector with an energy deposition of 311 keV and was absorbed in segment No. 17 of the box detector. The energy resolution was determined to be 40 keV (FWHM). The 311-keV energy deposition indicated an emission angle of 63° with respect to the surface of the stop detector. This value is in agreement with the range of 3° to 70° estimated from the geometrical arrangement of the detectors.

The α decay was followed by an sf event with a lifetime of 86.4 ms ($T_{1/2} = 60^{+290}_{-27}$ ms). The energy of the sf event was determined as a sum of the energies measured in the stop detector, 134 MeV, and in segment No. 21 of the box detector, 24 MeV. The measured total energy of 158 MeV was corrected for pulse height defects and energy loss of the escaped fragment in the dead layer of the detectors. The correction energy was determined to be 46 MeV, as discussed before. We obtained 204 MeV for the TKE value of the sf event.

The sf event was in coincidence with a γ-ray event of 749 keV in one of the crystals (Ge1) of the clover detector, which gives additional support for assigning it as a true sf event.

After having established the decay chain consisting of an α decay and subsequent sf, we searched for the recoil implantation preceding the α decay. Within a time window of 10.0 s we found nine candidates, on the average one every 1.1 s, which had the expected energies and time-of-flight values. Searching backward in time from the α decay, implantations were measured at 0.54, 1.40, and 1.64 s before the α decay. The position values obtained from the top connection agreed to within ± 1 mm of the mean value from the α decay and the sf event, as shown in Fig. 1. However, the bottom positions were larger by 1.6 mm, obviously owing to the low bottom position measured for the low energy of the escaped α particle of only 311 keV.

The analysis showed that, owing to the relatively high counting rate of background particles in this experiment, the correct recoil nucleus cannot be determined unambiguously using only the measured data. However, based on the measured data and the following arguments, we assign the observed event to the decay of the isotope ^{268}Hs.

In the first step we use the α energy of 9479 ± 16 keV ($Q_\alpha = 9623 \pm 16$ keV) to determine a half-life. Applying the three-parameter formula given in Ref. [30] [Eqs. (4) and (4a)], we obtain $T_{1/2} = 0.39 \pm 0.04$ s. The error bars are attributable to the energy uncertainty. It was shown in Ref. [30], that with this formula the experimental half-lives of even-even nuclei are reproduced to within a factor of 1.3. With respect to the theoretical half-life, the probability of observing α decay after 1.40 and 1.64 s of the recoil implantation is 8% and 5%, respectively. Therefore, recoil candidates two and three with half-lives of $0.97^{+4.64}_{-0.44}$ and $1.14^{+5.46}_{-0.52}$ s, respectively, can already be excluded with high probability. Good agreement is obtained with the half-life of $0.38^{+1.8}_{-0.17}$ s ($\tau = 0.54$ s) of the implantation directly preceding the α decay.

Second, we compare the measured α energy with the systematics of experimental as well as theoretical data [31]. Figure 2 shows that the experimental Q_α values of the

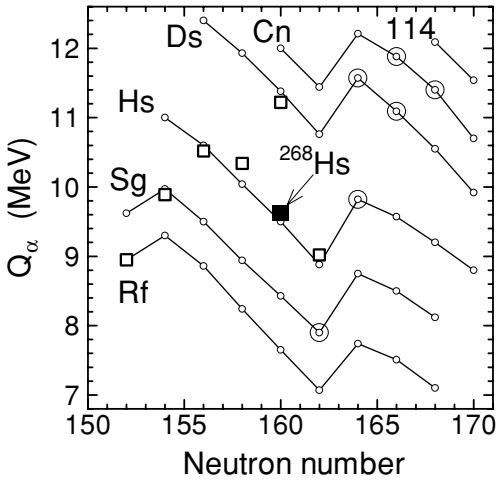

FIG. 2. α-decay Q values of even-even nuclei in the region of the single-particle energy gap for neutrons at $N = 162$. Open circles connected with lines represent calculated values [31]. Experimental values are marked with open squares. The Q_α value of the new isotope ^{268}Hs is marked with the solid square. Double circles represent calculated Q_α values of nuclei and their daughter products, which could be studied in experiments using the reactions ^{34,36}S + ^{248}Cm,^{244}Pu, and $4n$-evaporation channels.

considered even-even nuclei are well reproduced by the theoretical values and that the value assigned to ^{268}Hs fits perfectly into the systematics.

The α-decay daughter, ^{264}Sg, was measured to undergo sf. A half-life of 68^{+37}_{-18} ms was determined as a mean value from five events measured in Ref. [9] and three events in Ref. [6]. The half-life of 60^{+290}_{-27} ms of our sf event is in perfect agreement with this value. Also in agreement is the TKE of 204 MeV of our event with measured values of 234 and 159 MeV [9] and 197 MeV [6] of ^{264}Sg and a value of 210 MeV expected for ^{264}Sg from the Viola formula [32].

Cross sections of the measured events are discussed in Sec. IV. Therefore, at this point we only mention that the cross section for production of the isotope ^{267}Hs at $E_{\text{c.m.}} =$ 163.0 MeV agrees in magnitude with the value calculated for the $5n$ evaporation channel (see the lower part in Fig. 3). The calculations reveal that at an energy reduced by 11 MeV, namely, 152.0 MeV, we expect maximum yield for the $4n$ evaporation channel and thus production of the isotope ^{268}Hs.

Finally, we should mention that one of the reasons given in Ref. [33] for the nonobservation of ^{268}Hs in the reaction ^{25}Mg + ^{248}Cm was that the half-life could be shorter than 0.5 s. This indeed results from our assignment.

In addition to the two events assigned to ^{267}Hs and ^{268}Hs, one recoil-sf event was observed in each of the irradiations at the two different beam energies. Owing to low fission energy and short half-life, we assign these events to the decay of fission isomers produced by nucleon transfer reactions. For completeness, we also list the measured data of these two events in the following.

At the beam energy of 5.53 MeV/u, an sf event was observed 2.15 ms after the recoil implantation at 12.8 MeV in strip No. 1. This event occurred during the beam pause. An

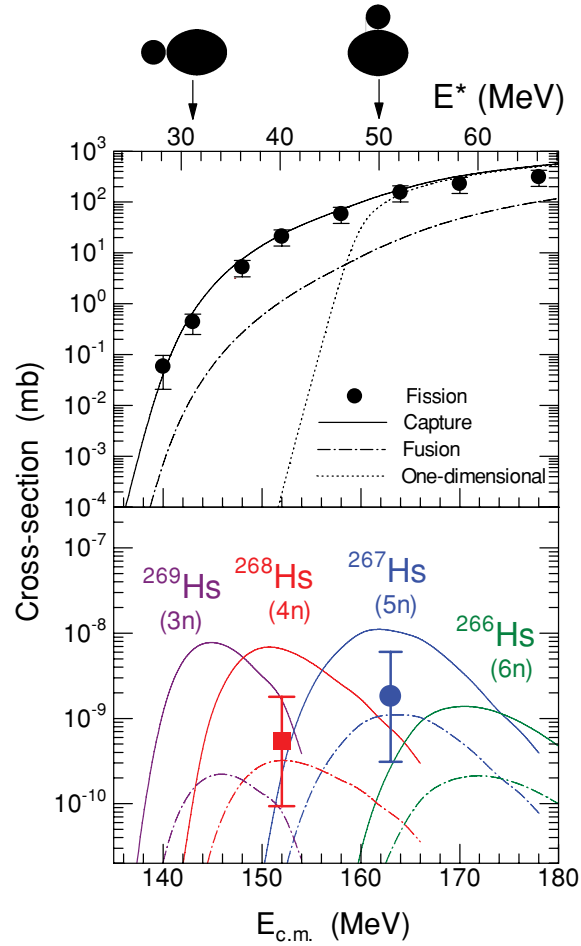

FIG. 3. (Color online) Experimental fission cross sections for FMT events of the reaction ^{34}S + ^{238}U as a function of the center-of-mass energy $E_{\text{c.m.}}$ and the excitation energy of the compound nucleus E^* (scale at the top). Coulomb barriers for polar and equatorial collisions are indicated by arrows. The solid line represents the capture cross sections σ_{cap} calculated by the CC code [34]. The dotted curve represents results of the one-dimensional barrier penetration model. The dash-dotted line is the calculated fusion cross sections σ_{fus} based on the Langevin description coupled with the CC model. (Bottom) Experimental cross sections for the production of ^{268}Hs (square) and ^{267}Hs (circle). Lines represent results of statistical model calculations for $3n$ to $6n$ evaporation channels based on different assumptions for fusion (see text for details).

energy deposit of 99 MeV was measured in the stop detector and one 29-MeV fragment was detected in the box detector. The resulting uncorrected energy sum is 128 MeV. The fission coincided with three γ rays from the Ge crystals.

The sf event at a beam energy of 5.16 MeV/u had a lifetime of 29 μs. It was also detected in strip No. 1 after a recoil implantation with an energy of 11.0 MeV. From the sf event a signal was obtained only from the stop detector at an energy of 104 MeV. Two γ rays were detected in coincidence.

The measured energies for both sf events in the stop detector, 99 and 104 MeV, respectively, are apparently smaller than the average of 197 MeV determined from 3 sf events of ^{264}Sg given in Refs. [6,9], 141 MeV from 3 events of ^{263}Sg [9], and 161 MeV from 16 events of ^{262}Sg [6,9]. This and

the short half-lives indicate that these two sf events originate from lighter nuclei, with high probability from fissioning shape isomers produced by nucleon transfer.

IV. RESULTS FROM IN-BEAM FISSION MEASUREMENT

The cross sections of the measured fragments are shown in Fig. 4 for five energies between $E_{\mathrm{c.m.}} = 148$ MeV and $E_{\mathrm{c.m.}} = 170$ MeV. The data analysis methods to determine the cross sections are the same as described in Ref. [19]. The half value of the integrated cross-section over the fragment mass gives the fission cross section. The obtained fission cross-sections are shown in the top panel of Fig. 3 together with the values obtained at $E_{\mathrm{c.m.}} = 140$, 143, and 178 MeV. In the following we compare the data to model calculations.

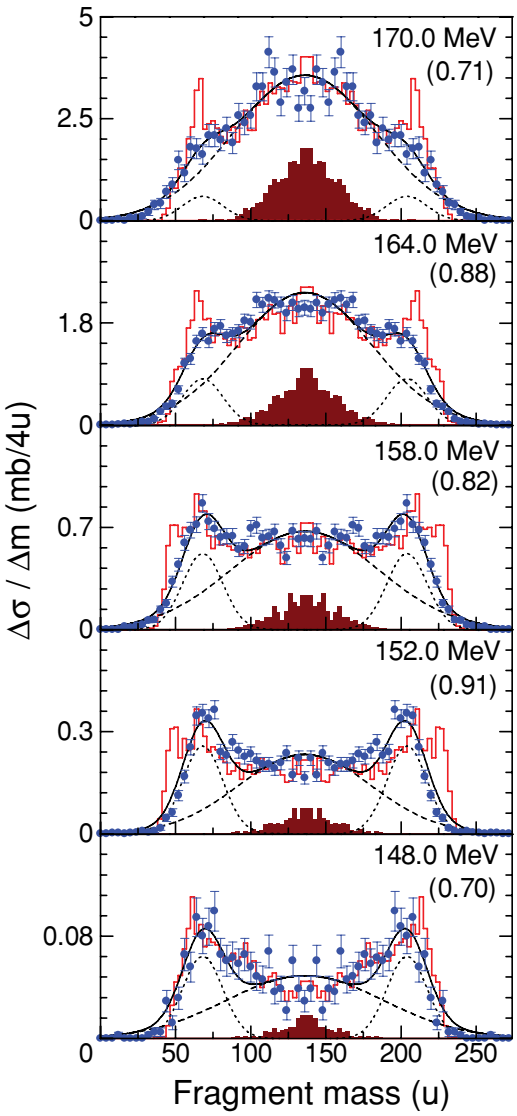

FIG. 4. (Color online) Mass distributions for FMT fission fragments for the reaction $^{34}\mathrm{S} + ^{238}\mathrm{U}$. Energies $E_{\mathrm{c.m.}}$ are given in each section of the figure. The data are disentangle in two parts, symmetric fission (dashed lines) and asymmetric fission (dotted lines). The sum of both components is given by the solid lines. The histograms show model calculations for FMT fission fragment distributions using the Langevin equation. The calculated fusion-fission parts are shown by the filled areas. The calculations were multiplied by the factor shown in parentheses such that the total cross section agrees with the experimental value to compare the shape of the mass distribution with the experiment.

The dotted line in the upper part of Fig. 3 represents results from a one-dimensional barrier penetration model. The calculation was performed using the CCDEGEN code [34]; however, nuclear deformation and coupling to excited states in the colliding nuclei were not taken into account. This relatively simple approach cannot explain the experimental data at energies below the barrier $E_{\mathrm{c.m.}} < 160$ MeV. Therefore, this model is no longer considered in the following discussion.

The solid line in Fig. 3 represents the results of coupled-channels (CC) calculation using the CCDEGEN code [34]. This model takes into account the deformation of ^{238}U with deformation parameters $\beta_2 = 0.275$ and $\beta_4 = 0.05$ [7] and the coupling to the 0.73-MeV 3^- state in ^{238}U and to the 2.13-MeV 2^+ state in ^{34}S [29]. The results of this calculation reproduce the data well in the entire energy region. The large enhancement of the cross sections in the sub-barrier region is attributed to the lowering of the Coulomb barrier in polar collisions with the deformed target nucleus ^{238}U.

In the second step, assuming fusion cross sections to be equal to the capture cross sections from the CC calculation, ER cross sections were calculated with the statistical model code HIVAP [35].

For testing purposes we used this approach for reproducing the known ER cross sections of ^{271,270,269}Hs ($3n$–$5n$ channels) produced in the reaction $^{26}\mathrm{Mg} + ^{248}\mathrm{Cm} \rightarrow ^{274}\mathrm{Hs}^*$ at excitation energies in the range $E^* = 36$–54 MeV [10,11]. Good agreement between experimental and calculated cross sections was obtained, which demonstrated that fusion cross sections are nearly equal to the capture cross sections in these kinds of asymmetric reactions.

Using the same set of parameters we then calculated the ER cross sections ($3n$–$6n$ channels) for the reaction $^{34}\mathrm{S} + ^{238}\mathrm{U} \rightarrow ^{272}\mathrm{Hs}^*$. The result is represented by the solid lines in the lower part of Fig. 3. A comparison with the experimental data shows, however, that the measured cross sections for ^{268}Hs ($4n$ channel) and ^{267}Hs ($5n$ channel) are overestimated by about one order of magnitude.

Two reasons could be responsible for the discrepancy. First, the fission probability of the compound nucleus $^{272}\mathrm{Hs}^*$ could be higher than in the case of the reference reaction with $^{274}\mathrm{Hs}^*$ as compound nucleus, or second, the fusion probability is reduced in comparison to the more asymmetric reference reaction.

We rule out the first argument because both compound nuclei differ by only two neutrons, and they and their subsequent residues after neutron evaporation are located in a region where the fission barriers vary only moderately with neutron number [36].

Therefore, we conclude that in our reaction the fusion process is reduced owing to fragment reseparation after FMT; this is still before a compound nucleus was formed. This so-called quasifission process should have a different fragment mass distribution compared to fission of the compound

nucleus, called as fusion-fission. Furthermore, it is found from a comparison of experimental and calculated ER cross sections (lower part in Fig. 3) that the reduction of fusion owing to quasifission is higher at an excitation energy of 40 MeV (^{268}Hs) than at 52 MeV (^{267}Hs).

The data points in the five panels in Fig. 4 show the change of the FMT fragment mass distribution with beam energy. To draw Fig. 4, we assumed that the mass distributions do not depend on the emission angle of the fragment in the center-of-mass system, $\theta_{\mathrm{c.m.}}$. At the highest energy of 170.0 MeV, the cross section has a maximum for a symmetric mass distribution with $A = 136$. With decreasing energy, an asymmetric mass distribution emerges with the peaks for light and heavy fragments centered on $A_{\mathrm{L}} = 68$ and $A_{\mathrm{H}} = 204$. At the lowest energy the spectrum is dominated by the asymmetric mass distribution. The asymmetric fission is connected to the fragments near the double-closed shell nuclei, ^{78}Ni and ^{132}Sn.

A similar observation was made in the study of the reaction $^{36}\mathrm{S} + ^{238}\mathrm{U} \rightarrow ^{274}\mathrm{Hs}^*$ [19]. In agreement with the conclusions drawn in Refs. [19,37,38], we assign the asymmetric mass distribution to the quasifission process.

Integral cross sections of the two components were determined by fitting three Gaussian curves to the data points shown in Fig. 4, the dashed curve for the symmetric component and the two dotted curves for the asymmetric one. The solid line shows the sum of both components. At energies of $E_{\mathrm{c.m.}} = 164$ and 152 MeV, where the isotopes ^{267}Hs and ^{268}Hs were measured, the fractions of the symmetric fission component relative to all FMT events are 0.83 and 0.60, respectively. However, the fractions of the measured ER cross sections for ^{267}Hs and ^{268}Hs relative to the calculated values (solid lines in the lower panel of Fig. 3) are $0.17^{+0.39}_{-0.14}$ and $0.083^{+0.19}_{-0.07}$, respectively. The calculated fusion-evaporation cross sections (solid lines in Fig. 3) are based on the assumption that all FMT events contribute to fusion. However, the experimental cross sections are significantly smaller. Therefore, we have to conclude that the assumption made before for the more asymmetric reaction $^{26}\mathrm{Mg} + ^{248}\mathrm{Cm}$ is not fulfilled for the reaction $^{34}\mathrm{S} + ^{238}\mathrm{U}$. This means that there also exists a significant contribution from quasifission to the symmetric mass distribution.

For a quantitative analysis of the two contributions to the mass symmetric fragment component, we performed a model calculation combining the CC method and a dynamical description of the reaction based on the three-dimensional Langevin equation [39].

The dynamical calculation based on the Monte Carlo method was used for describing the reaction paths in the potential energy landscape. The calculation started at the contact configuration. The deformation of the reaction partners and their statistical orientation in the reaction plane was considered. The CC method was first used to compute the penetration probability of the Coulomb barrier for a fixed orientation angle. The dynamical calculation was then started from the shape at contact configuration for each orientation. Fusion is defined as the case when a compound nucleus is formed. Quasifission occurs when the system disintegrates before a compound nucleus forms. The calculated distributions of FMT fragments (sum of fusion-fission and quasifission) as a function of the center-of-mass energy are represented by the histograms in Fig. 4. The calculated cross section are in good agreement with the measured data.

The pronounced peaks in the calculated mass distribution at $A_{\mathrm{H}} = 209$ and $A_{\mathrm{L}} = 63$ at $E_{\mathrm{c.m.}} = 170.0$ and 164.0 MeV are attributable to shell effects of the fragments. These narrow peaks, however, are not observed in the experimental data because of insufficient mass resolution of FWHM = 8.5 u.

The calculated distributions of fragments from fusion-fission are shown by the filled areas in Fig. 4. Apparently, the widths of these distributions are narrower; standard deviations are less than half the widths obtained by the fitting procedure to all symmetric FMT events.

Also, the calculated integrated cross sections of fusion-fission events are much lower than those obtained from the data fitting procedure. At the center-of-mass energies of 164 and 152 MeV, the cross-section ratios are 0.10 and 0.049, respectively.

Fusion cross sections, σ_{fus}, calculated with this model are shown as a dashed-dotted line in the top panel of Fig. 3. The σ_{fus} is about one order of magnitude below the data points representing the capture cross section, σ_{cap}. However, the ratio $\sigma_{\mathrm{fus}}/\sigma_{\mathrm{cap}}$ increases toward higher bombarding energies. The calculation demonstrates the orientation effects of a compact configuration at nuclear contact resulting in a larger fusion probability. Using these fusion-fission cross sections, we calculated new ER cross sections shown by the dash-dotted lines in the bottom panel of Fig. 3. Obviously, the Langevin description coupled with the CC model reproduces the measured ER cross sections reasonably well.

The standard deviation of the symmetric mass distribution for the reaction $^{34}\mathrm{S} + ^{238}\mathrm{U}$ as obtained by the fitting procedure is about ∼65% larger than the value obtained for the recently studied reaction $^{30}\mathrm{Si} + ^{238}\mathrm{U}$ [40]. This increase of the width when using heavier projectiles suggests a different source contributing to the symmetric fragment distribution than fusion-fission.

The presence of a quasifission channel in the symmetric mass region was argued from measurements of fission fragment properties in the reaction $^{32}\mathrm{S} + ^{232}\mathrm{Th}$ [41]. The fragment mass-angle correlations as well as the larger fragment anisotropy than that predicted by the transition state model were attributed to the occurrence of quasifission also in the symmetric fragment region.

In spite of the increasingly reduced fusion probability for production of SHN using heavier projectiles, our cross-section calculations reveal a considerable yield for producing relatively neutron-rich nuclei at energies below the Bass barrier, when targets of deformed actinide nuclei are used. Figure 3 shows the calculated cross section for ER produced in a $3n$ evaporation channel (^{269}Hs). In this reaction, the cross section is expected to be comparable to that for producing ^{268}Hs in the $4n$ channel.

Using the reaction energy below the Bass barrier, the new isotopes $^{274-277}$Ds, $N = 164$–167, could be produced in the reactions $^{34,36}\mathrm{S} + ^{244}\mathrm{Pu}$ in $3n$–$4n$ evaporation channels or $^{278-281}$Cn, $N = 166$–169, in $^{34,36}\mathrm{S} + ^{248}\mathrm{Cm}$ reactions also in

$3n$–$4n$ channels. α decay from these nuclei would populate isotopes of hassium and seaborgium, from which the isotopes ^{272,273}Hs, $N = 164$ and 165, and ^{268,269}Sg, $N = 162$ and 163, would be identified.

Isotopes of odd elements could be produced in reactions with ^{34,36}S beams and an ^{243}Am target. At present the isotopes ^{273,275,276}Rg, $N = 162$, 164, and 165, and their daughter nuclei ^{269,271,272}Mt, $N = 160$, 162, and 163, are not yet known.

Using the methods described earlier, we calculated the fusion-evaporation cross sections for some of the suggested reactions. The fusion probabilities change only slightly with the atomic number of the target nuclei. For example, in the reactions ^{34}S + ^{238}U, ^{244}Pu, and ^{248}Cm fusion probabilities at the Bass barriers are 0.096, 0.079, and 0.057, respectively. Using these data we obtained, for the fusion-evaporation cross sections for producing of ^{275}Ds and ^{274}Ds in $3n$ and $4n$ channels of the reaction ^{34}S + ^{244}Pu, values of 30 and 20 fb, respectively. These values are significantly lower than in the case of the same evaporation channels in the reaction ^{34}S + ^{238}U. The reason for this is the predicted lower fission barrier, which was estimated in the following way. For these heavy nuclei the liquid-drop part of the barrier is almost zero; thus, the barrier is determined dominantly by the ground-state shell correction energy, which was obtained by subtracting the liquid-drop mass taken from Ref. [42] from a predicted mass. For the predicted mass we referred to the theoretical masses of Ref. [43]. However, we modified them systematically in such a way that the experimental masses given in Ref. [44] were optimally reproduced.

The survival probability for compound nuclei at $Z = 110$ and $N = 168$ is lower than in the case of $Z = 108$ and $N = 164$. Nuclei in this region are known to be α emitters [1]; however, the height of their fission barriers is rather uncertain [36,45]. Therefore, experimental cross-section data would provide valuable information on the extension into the heavier-element region of shell-stabilized deformed nuclei centered on $Z = 108$ and $N = 162$ and the beginning of spherical SHN predicted around $Z = 114$ and $N = 184$. Between these two regions minimum cross sections must be expected, which will be determined dominantly by the height of the fission barrier of these nuclei.

The same argument holds for the synthesis of new isotopes of odd elements using the reaction ^{36}S + ^{243}Am. Based on the relatively low fission barriers determined by the procedure mentioned earlier, cross sections of 40 and 7 fb were obtained for production of ^{276}Rg and ^{275}Rg in $3n$ and $4n$ evaporation channels, respectively.

The knowledge of synthesis and decay properties of the nuclei discussed earlier is especially important for three reasons. First, they build a bridge between the well established, but relatively neutron-deficient nuclei produced in cold-fusion reactions and those with higher neutron number produced in hot fusion, which are not, however, connected to known nuclei, because their α-decay chains end in a region of spontaneously fissioning nuclei. Second, the α-decay Q values of these new nuclei, together with the Q values of those already known, would provide information on the strength of the predicted increased binding energy at $Z = 108$ and $N = 162$. As a result of large gaps in the single-particle energies, increased Q_α values are expected for nuclei beyond these neutron and proton numbers. In Fig. 2 the predicted Q_α values of the so-far-unknown nuclei are marked by double circles. However, owing to the high energies of 11–12 MeV, half-lives close to the detection limit of 1 μs must be expected for some of the nuclei [31]. Third, fusion-evaporation cross sections will provide information on the variation of the fission barriers and the location of an expected minimum in the transitional region between deformed heavy nuclei and spherical SHN.

V. CONCLUSION AND OUTLOOK

The reaction ^{34}S + ^{238}U was studied to obtain information on the fusion probability at energies below and above the fusion barrier. Experiments on production and identification of ERs were performed at the velocity filter SHIP. Decay properties of the isotope ^{267}Hs were confirmed, and the new isotope ^{268}Hs was identified. The measured α-decay Q value of this even-even nucleus with 108 protons and 160 neutrons agrees well with the results of theoretical calculations for deformed nuclei. These nuclei are located in a region where increased stability is predicted owing to large gaps in the single-particle energies at $N = 162$ and $Z = 108$.

In-beam fission fragment mass distributions were studied for the same reaction at the JAEA tandem accelerator. In comparison with more asymmetric reactions, it was shown that the relatively wide distribution assigned to symmetric fission has two components. To explain the measured ER cross sections, a relatively large fraction of symmetric quasifission events, even larger than fusion-fission events, had to be assumed.

The measured fragment mass distributions were reproduced by the model calculations based on the three-dimensional Langevin equation taking into account orientation effects of the deformed target nuclei. In combination with the statistical model code, the cross sections for ERs were calculated. These data were in good agreement with the measured cross sections for the production of ^{267}Hs and ^{268}Hs.

The theoretical model was used for calculating cross sections for synthesis of heavy nuclei in reactions not studied so far. It was shown that the cross sections for reactions at low beam energy are in a range that allows these nuclei to be studied using presently available techniques. With beams of ^{34,36}S and targets of ^{244}Pu, ^{231}Am, and ^{248}Cm it seems possible that 18 new isotopes could be produced in $3n$ and $4n$ evaporation channels, which are located in the region of elements from seaborgium to copernicium with neutron numbers $\geqq$162 so that the gap between the known nuclei produced in cold and hot fusion reactions could be filled. Cross-section data will provide information on the height of the fission barriers of nuclei in this transitional region.

ACKNOWLEDGMENTS

We thank the UNILAC staff and the crew of the JAEA tandem accelerator facility for preparation of stable and/or

intense ^{34}S beams. We are grateful to W. Hartmann and J. Steiner of the GSI target laboratory for manufacturing the targets, H. G. Burkhard for taking care of the mechanical devices at SHIP, and J. Maurer for the electrical devices at SHIP. S.H. is much indebted to the Josef Buchmann-Foundation for financial support. S.A. was supported by the Slovak Research and Development Agency (Contract No. APVV-20-006205). This work was supported by a Grant-in-Aid for Scientific Research of the Japan Society for the Promotion of Science.

[1] Yu. Ts. Oganessian, J. Phys. G **34**, R165 (2007).
[2] S. Hofmann and G. Münzenberg, Rev. Mod. Phys. **72**, 733 (2000).
[3] K. Morita *et al.*, J. Phys. Soc. Jpn. **73**, 1738 (2004).
[4] K. Nishio, H. Ikezoe, S. Mitsuoka, K. Satou, and S. C. Jeong, Phys. Rev. C **63**, 044610 (2001).
[5] S. Mitsuoka, H. Ikezoe, K. Nishio, K. Satou, and J. Lu, Phys. Rev. C **65**, 054608 (2002).
[6] K. Nishio *et al.*, Eur. Phys. J. A **29**, 281 (2006).
[7] K. Nishio *et al.*, Phys. Rev. Lett. **93**, 162701 (2004).
[8] J. M. Gates *et al.*, Phys. Rev. C **77**, 034603 (2008).
[9] K. E. Gregorich *et al.*, Phys. Rev. C **74**, 044611 (2006).
[10] J. Dvorak *et al.*, Phys. Rev. Lett. **97**, 242501 (2006).
[11] J. Dvorak *et al.*, Phys. Rev. Lett. **100**, 132503 (2008).
[12] S. Hofmann *et al.*, GSI Nachr. **02-1995**, 4 (1995).
[13] S. Hofmann, Rep. Prog. Phys. **61**, 639 (1998).
[14] Yu. A. Lazarev *et al.*, Phys. Rev. Lett. **75**, 1903 (1995).
[15] R. Mann *et al.*, GSI Sci. Rep. **2003**, 224 (2004).
[16] S. Saro, Nucl. Instrum. Methods A **381**, 520 (1996).
[17] S. Hofmann *et al.*, Eur. Phys. J. A **32**, 251 (2007).
[18] K. Nishio *et al.*, AIP Conf. Proc. **891**, 71 (2007).
[19] K. Nishio *et al.*, Phys. Rev. C **77**, 064607 (2008).
[20] R. Bass, Nucl. Phys. A **231**, 45 (1974).
[21] S. Hofmann *et al.*, Eur. Phys. J. A **32**, 251 (2007).
[22] S. Hofmann, J. Nucl. Radiochem. Sci. **4**, R1 (2003).
[23] T. N. Ginter *et al.*, Phys. Rev. C **67**, 064609 (2003).
[24] K. Morita *et al.*, Eur. Phys. J. A **21**, 257 (2004).
[25] C. M. Folden III *et al.*, Phys. Rev. Lett. **93**, 212702 (2004).
[26] K.-H. Schmidt *et al.*, Z. Phys. A **316**, 19 (1984).
[27] A. Ghiorso *et al.*, Phys. Rev. Lett. **33**, 1490 (1974).
[28] K. E. Gregorich, M. R. Lane, M. F. Mohar, D. M. Lee, C. D. Kacher, E. R. Sylwester, and D. C. Hoffman, Phys. Rev. Lett. **72**, 1423 (1994).
[29] R. B. Firestone *et al.*, *Table of Isotopes* (John Wiley & Sons, New York, 1998), 8th ed.
[30] A. Parkhomenko and A. Sobiczewski, Acta Phys. Pol. B **36**, 3095 (2005).
[31] I. Muntian *et al.*, Acta Phys. Pol. B **34**, 2073 (2003).
[32] V. E. Viola, Jr., Nucl. Data Sheets, Sec. A **1**, 391 (1966).
[33] J. Dvorak *et al.*, Phys. Rev. C **79**, 037602 (2009).
[34] Modified version of the CCFULL code, K. Hagino *et al.*, Comput. Phys. Commun. **123**, 143 (1999).
[35] W. Reisdorf and M. Schädel, Z. Phys. A **343**, 47 (1992).
[36] R. Smolanczuk, J. Skalski, and A. Sobiczewski, Phys. Rev. C **52**, 1871 (1995).
[37] M. G. Itkis *et al.*, Nucl. Phys. A **787**, 150c (2007).
[38] G. N. Knyazheva *et al.*, Phys. Rev. C **75**, 064602 (2007).
[39] Y. Aritomo *et al.* (unpublished).
[40] K. Nishio *et al.* (submitted to Phys. Rev. C).
[41] D. J. Hinde, R. duRietz, M. Dasgupta, R. G. Thomas, and L. R. Gasques, Phys. Rev. Lett. **101**, 092701 (2008).
[42] W. D. Myers and W. J. Swiaecki, Ark. Phys. **36**, 343 (1967).
[43] P. Möller *et al.* At. Data Nucl. Data Tables **59**, 185 (1995).
[44] G. Audi and A. H. Wapstra, Nucl. Phys. A **595**, 409 (1995).
[45] P. Möller, A. J. Sierk, T. Ichikawa, A. Iwamoto, R. Bengtsson, H. Uhrenholt, and S. Aberg, Phys. Rev. C **79**, 064304 (2009).